KeAi

CHINESE ROOTS
GLOBAL IMPACT

Contents lists available at ScienceDirect

Petroleum Science

journal homepage: www.keaipublishing.com/en/journals/petroleum-science



Original Paper

Magnetically controlled self-sealing pressure-preserved coring technology



Gui-Kang Liu ^a, He-Ping Xie ^{a, b}, Cong Li ^{a, *}, Zhen-Xi You ^c, Xiao-Jun Shi ^a, Jian-Jun Hu ^b, Ming-Zhong Gao ^{a, b}

- ^a State Key Laboratory of Intelligent Construction and Healthy Operation and Maintenance of Deep Underground Engineering, College of Water Resource and Hydropower, Sichuan University, Chengdu, 610065, Sichuan, China
- ^b Guangdong Provincial Key Laboratory of Deep Earth Sciences and Geothermal Energy Exploitation and Utilization, Institute of Deep Earth Sciences and Green Energy, College of Civil and Transportation Engineering, Shenzhen University, Shenzhen, 518060, Guangdong, China
- ^c School of Mechanical Engineering, Sichuan University, Chengdu, 610065, Sichuan, China

ARTICLE INFO

Article history: Received 18 July 2023 Received in revised form 29 April 2024 Accepted 7 May 2024 Available online 12 May 2024

Edited by Jia-Jia Fei

Keywords:
In situ pressure-preserved coring
Magnetically controlled
Self-sealing
Magnetic design
Deep earth exploration

ABSTRACT

Pressure-preserved coring is an effective means to develop deep resources. However, due to the complexity of existing pressure-preserved technology, the average success rate of pressure-preserved coring is low. In response, a novel in situ magnetically controlled self-sealing pressure-preserved coring technology for deep reserves has been proposed and validated. This innovative technology distinguishes itself from conventional methods by employing noncontact forces to replace traditional pretensioning mechanisms, thereby enhancing the mechanical design of pressure-preserved coring equipment and significantly boosting the fault tolerance of the technology. Here, we report on the design, theoretical calculations, experimental validation, and industrial testing of this technology. Through theoretical and simulation calculations, the self-sealing composite magnetic field of the pressure controller was optimized. The initial pre-tensioning force of the optimal magnetic field was 13.05 N. The reliability of the magnetically controlled self-sealing pressure-preserved coring technology was verified using a self-developed self-sealing pressure performance testing platform, confirming the accuracy of the composite magnetic field calculation theory. Subsequently, a magnetically controlled self-triggering pressure-preserved coring device was designed. Field pressure-preserved coring was then conducted, preliminarily verifying the technology's effective self-sealing performance in industrial applications. Furthermore, the technology was analyzed and verified to be adaptable to complex reservoir environments with pressures up to 30 MPa, temperatures up to 80 °C, and pH values ranging from 1 to 14. These research results provide technical support for multidirectional pressure-preserved coring, thus paving a new technical route for deep energy exploration through coring.

© 2024 The Authors. Publishing services by Elsevier B.V. on behalf of KeAi Communications Co. Ltd. This is an open access article under the CC BY-NC-ND license (http://creativecommons.org/licenses/by-nc-nd/4.0/).

1. Introduction

With the deeper development of underground energy sources, such as oil, coalbed methane, natural gas, and other resources, addressing the exploration and safe development of resources has become a major strategic issue (Xie et al., 2017, 2021a; Gong et al., 2020; Hu et al., 2021; Gao et al., 2022; Zou et al., 2022; Guo et al., 2023a). Pressure-preserved coring is one of the most intuitive and reliable methods used in deep resource exploration technology

* Corresponding author. E-mail address: licong@scu.edu.cn (C. Li). (Xie et al., 2020; Gladenkov and Gladenkov, 2021; Wang H.G. et al., 2022; Wang et al., 2022b). Pressure-preserved coring technology significantly enhances the accuracy and reliability of measuring critical parameters, including gas pressure and fluid saturation, compared to conventional coring methods (Sun et al., 2019). Pressure-preserved coring technology is mainly applied to natural gas, shale gas, coalbed methane, natural gas hydrate, and oil (Fu et al., 2020; Wang et al., 2020; Zhou et al., 2022). For example, as early as the 1980s, PCB (Pressure Core Barrel) pressure-preserved coring technology was developed in the USA and successfully applied to coring sites (Kvenvolden and Cameron, 1983). PCS (Pressure Core Sampler) pressure-preserved coring technology was

List of symbols

the magnetic scalar potential, A $\varphi_{\rm m}$ the normal vector of the solution domain, 1 n В the magnetic flux density of the solution domain, ${\it \textbf{B}}_{in~(i=1,2,3~\dots)}$ the magnetic flux density of the boundary of the solution domain, T $\mathbf{\textit{H}}_{i_{t}\ (i=1,2,3\ ...)}$ the magnetic field strength of the boundary of the solution domain, T the relative permeability, 1 μ_0 the permeability of vacuum, H/m μ_{Γ} B. the remanence magnetic strength, T the magnetic force on the valve cover, N $\boldsymbol{F}_{\mathrm{m}}$ f the magnetic force on a unit. N е the normal vector, 1 pressure of the target reservoir, MPa P the acceleration due to gravity, 9.81 m/s² g density of the drilling fluid in the reservoir, kg/m³ ρ depth of the target reservoir, m h

developed by Pettigrew, who successfully obtained a pressurepreserved sample (Pettigrew, 1992). In the early 21st century, German scientists (Abegg et al., 2008) developed two pressurepreserved devices, the MAC (Multiple Autoclave Corer) and the DAPC (Dynamic Autoclave Piston Corer), which have been successfully used in maritime applications. Pressure-preserved and gas-preserving coring devices and complementary technology were developed by Gao's team (Gao M.Z. et al., 2021). A coalbed methane coring device with thermal insulation and the capacity to maintain the core pressure and shape was developed by Wang et al. based on ball valves (Wang X.G. et al., 2021). Moreover, the GW-CP194-80A pressure-maintaining coring device was developed by the China National Petroleum Corporation (Yang et al., 2020). A gas hydrate coring device with heat-retention and pressure-preserved capacity was developed by the China Petroleum and Chemical Corporation (Ren, 2020). Thin-walled pressure-retaining coring devices for seafloor drills were developed by the Hunan University of Science and Technology (Wang et al., 2022a). The core pressurepreserved control device in the above pressure-preserved coring technology mainly includes ball valves (Kubo et al., 2014) and flap valves (Chen et al., 2013; He et al., 2019; Li et al., 2022). Considering sealing, pressure-preserved capacity, and application, the flap valve is the most promising pressure-preserved controller (Xie et al., 2021b). Therefore, the pressure-preserved controllers described below are flap valve structures.

The initial self-sealing of the flap valve relies mainly on the impact force generated by the release of the sealed spring sleeve and the elastic force of the spring after pressing to produce a sealing-specific pressure (see Fig. 1).

At this point, the elastic force is called the initial sealing force (Li et al., 2021). However, this sealing method has several drawbacks.

1) Impact damage on the back of the valve cover affects its service life. 2) When drilling vertically upward, the sealed spring sleeve may not be released in time and may affect the pressure effect. 3) The wear of the clamp mechanism of the sealed spring sleeve will make it possible to release it in advance, causing the valve cover to be stuck by the sealed spring sleeve before closing so that the pressure cannot be preserved. Due to the limited internal space of the coring device, the traditional mechanical seal method lacks sufficient space, so it is envisaged to use a noncontact force instead of the elastic force generated by the spring sleeve. The pressure-

preserved controller must achieve initial self-sealing without changing the internal space or size of the original coring device. Noncontact forces include gravity, electromagnetic forces, strong nuclear forces, and weak nuclear forces, and electromagnetic forces are most likely to act as the initial sealing force. Therefore, Xie's team (Liu et al., 2023) first proposed the use of magnetically controlled self-sealing pressure-preserved coring technology (Fig. 2). The triggering permanent magnet generates a repulsive force with the valve cover. When the valve cover lifts the limit, the repulsive force will push the valve cover to start triggering. When the valve cover rotates to a certain angle, the permanent magnet on the valve seat attracts it, facilitating faster closure. This approach employs magnetic force to achieve the initial self-sealing of the pressure-preserved controller following the coring process.

In summary, a pressure-preserved controller based on magnetic control was innovatively designed by focusing on solving the self-sealing problem of pressure-preserved controllers. This study provides a theoretical basis for the principle and technology of in situ pressure coring of deep resources and provides a new coring technique for deep energy exploration and scientific drilling.

2. Principle and design

2.1. Magnetic control self-sealing principle

The main sealing components of the magnetically controlled self-sealing pressure-preserved controller include three parts: a stable magnetic field source, sealing paramagnetic main components, and a sealing ring. The magnetic force generated by the magnetic field source is used to provide the pre-tightening force so that there is an initial sealing pressure between the sealing surfaces to achieve initial self-sealing. The principle is shown in Fig. 3.

The pressure-preserved process can be divided into two stages. In the first stage, the valve cover acts as a magnetic field source or generates a magnetic force after being magnetized. At this time, the sealing ring between the valve cover and the valve seat will be squeezed by magnetic force, and the very small pores on the sealing surface will be filled so that the in situ pressure inside the pressure-preserved cabin body will not leak through these very small cracks. In the second stage, the pressure of the external environment gradually decreases and forms a pressure difference with the inside of the pressure-preserved cabin body. The internal pressure of the pressure-preserved cabin body gradually increases, the valve cover is increasingly tightly pressed, and the deformation of the sealing ring increases. Therefore, as long as the initial self-sealing is effective, the pressure-preserved controller performs well.

2.2. Structural design of the pressure-preserved controller under magnetic control

The magnetic field of the designed pressure-preserved controller is located below its sealing surface, and a fan-shaped slot is machined around the circumference of the valve seat. To ensure the strength of the valve seat, the slot thickness is taken as half the thickness of the valve seat itself. Fan-shaped permanent magnets with different magnetic field directions are placed in the fan-shaped slot to form a composite magnetic field to that of the magnetic force. The basic size of the pressure-preserved controller is shown in Fig. 4.

According to the study, a combination of multiple permanent magnets does not necessarily produce a stronger magnetic field (Liu et al., 2020). Thus, in this article, 1–4 permanent magnets are designed in the valve seat. The fan-shaped slot can be arranged outside or inside the valve seat. The specific scheme is shown in Figs. 5 and 6. In the figures, the left side is the three-dimensional

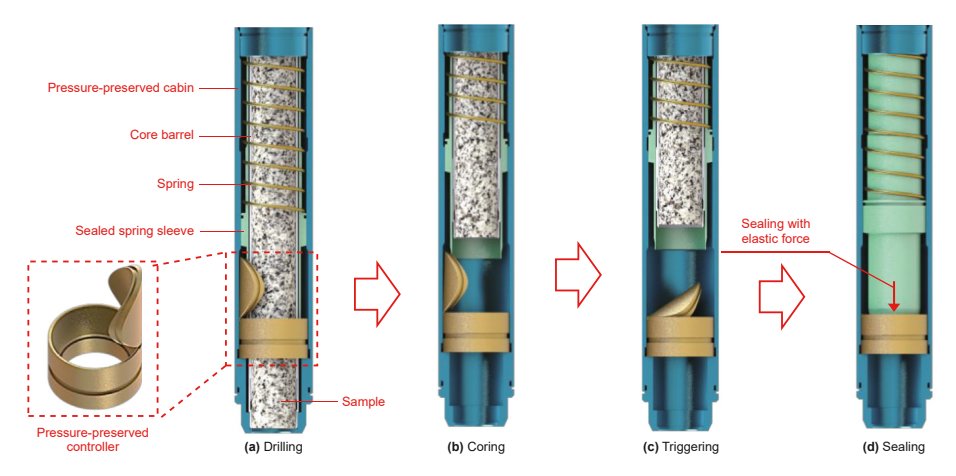


Fig. 1. Pressure-preserved principle of the pressure-preserved controller.

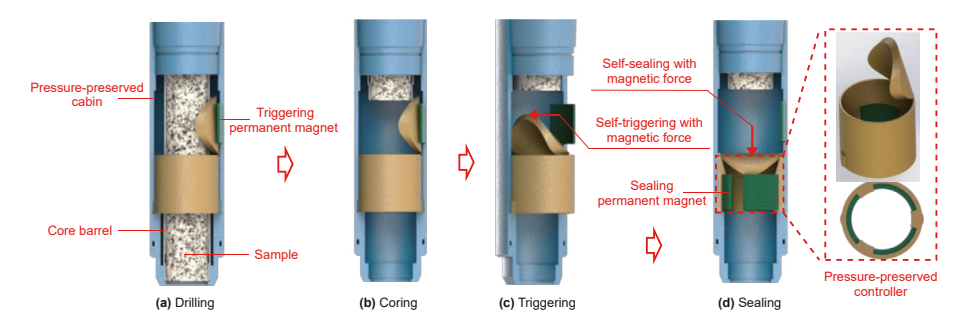


Fig. 2. Magnetically controlled self-sealing pressure-preserved coring technology.

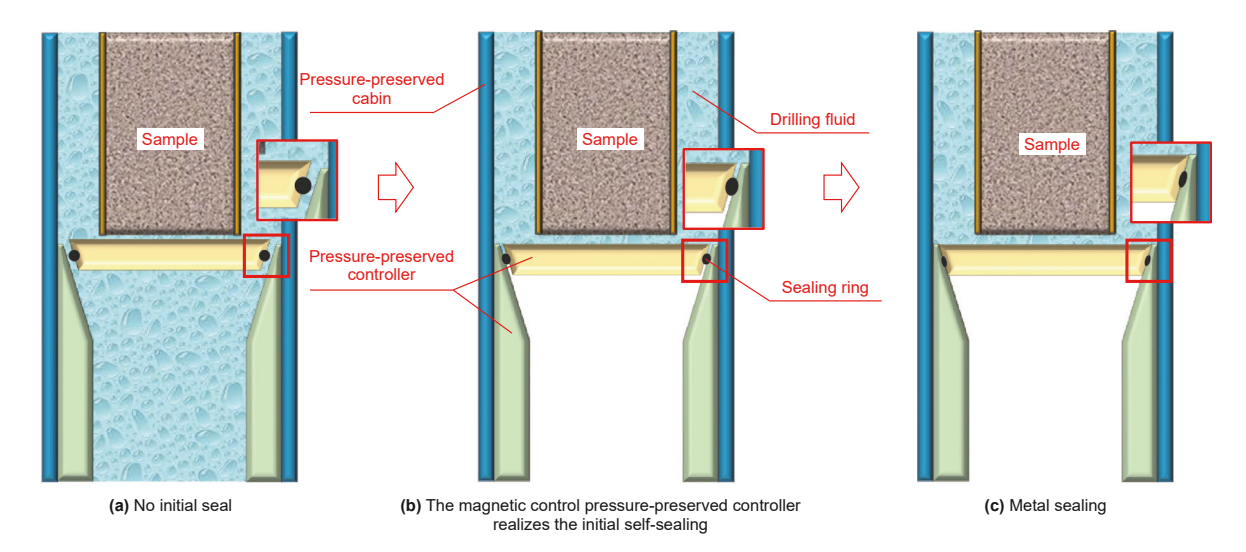


Fig. 3. Working principle of pressure-preserved controller sealing.

diagram of the valve seat, and the right side is the plan of the magnetic field arrangement of the valve seat. Gray represents the permanent magnet, and yellow represents the valve seat.

2.3. Magnetic circuit design

2.3.1. Composite magnetic field design

There are three magnetic field directions of the fan-shaped permanent magnet, which are radial, axial and circumferential, as shown in Fig. 7.

According to the magnetization method, the cylindrical coordinate system is introduced, as shown in Fig. 8. The three axes correspond to three magnetization modes, where the a-axis represents axial magnetization, the p-axis represents circumferential magnetization, and the r-axis represents radial magnetization. Using ri, pi, and ai to represent the magnetization of each tile permanent magnet, i represents the number of permanent magnets that the valve seat can integrate, $i \in (1,2,3,4)$. The unit vectors of the three axes can represent the magnetization direction of each magnet, and the values of ri, pi and ai can be represented by 0 or 1.

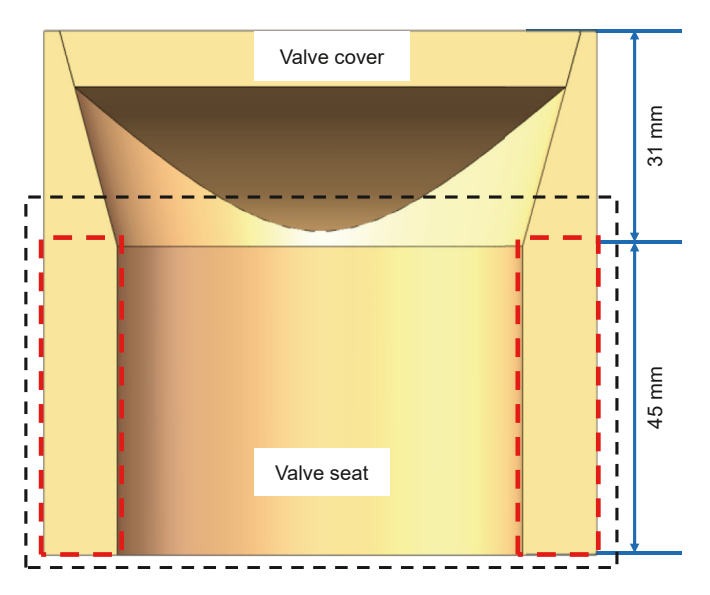


Fig. 4. Basic size of the pressure-preserved controller.

Between them, 0 represents unmagnetized, and 1 represents magnetized. For example, when there are two identical axially magnetized permanent magnets on the valve seat, it can be represented by 2a. At this time, the values of a1 and a2 are both 1, while the values of r1, r2, p1, and p2 are 0. The combination of magnetic circuits is arranged according to this rule.

When there is one permanent magnet in the valve seat, there are two magnetic fields. The axial magnetization and radial magnetization are shown in Table 1.

When there are two permanent magnets in the valve seat, there are six kinds of composite magnetic fields. Among them, there are three same-direction magnetic field schemes and three combined magnetic field schemes, which are 2r, 2p, 2a, rp, ra, and pa, as shown in Table 2.

When there are three permanent magnets in the valve seat,

there are ten kinds of composite magnetic fields. Among them, there are three identical magnetic field schemes, six combined magnetic field schemes (two magnetic field directions), and one multiple magnetic field scheme (three magnetic field directions), which can be written as 3r, 3p, 3a, 2rp, 2ra, r2p, r2a, p2a, 2pa, and rpa, as shown in Table 3.

When there are four permanent magnets in the valve seat, there are twenty-one kinds of composite magnetic fields. There are three identical magnetic field schemes, twelve combined magnetic field schemes (two magnetic field directions), and six multiple magnetic field schemes (3 magnetic field directions), which can be written as 4r, 4p, 4a, 3rp, 2r2p, rprp, r3p, 3ra, 2r2a, rara, r3a, 3pa, 2p2a, papa, p3a, rp2a, rapa, r2pa, rpap, 2rpa, and rpra, as shown in Table 4.

2.3.2. Valve cover material and its magnetization direction design

The use of permanent magnets as the processing material of the valve cover increases the magnetic field strength of the system to ensure greater magnetic force. There are two directions of the magnetic field of the valve cover, as shown in Fig. 9. The arrows in the figure indicate the magnetic field direction. A positive magnetization indicates that the magnetic field direction is consistent with the magnetic attraction direction of the valve cover, and a reverse magnetization indicates that the magnetic field direction is opposite to the magnetic attraction direction of the valve cover.

3. Simulation analysis of the sealing characteristics

3.1. Preparation

Through SolidWorks modeling software and COMSOL Multiphysics simulation software joint analysis, an AC/DC physical field is established, and a steady-state field is selected as the solution research configuration. The boundary formula of the solution domain includes the hypothesis equation of magnetic insulation and the hypothesis equation of zero magnetic scalar potentials. It also includes the magnetic field relationship between the magnetic conduction domains, which can be expressed by Eq. (1).

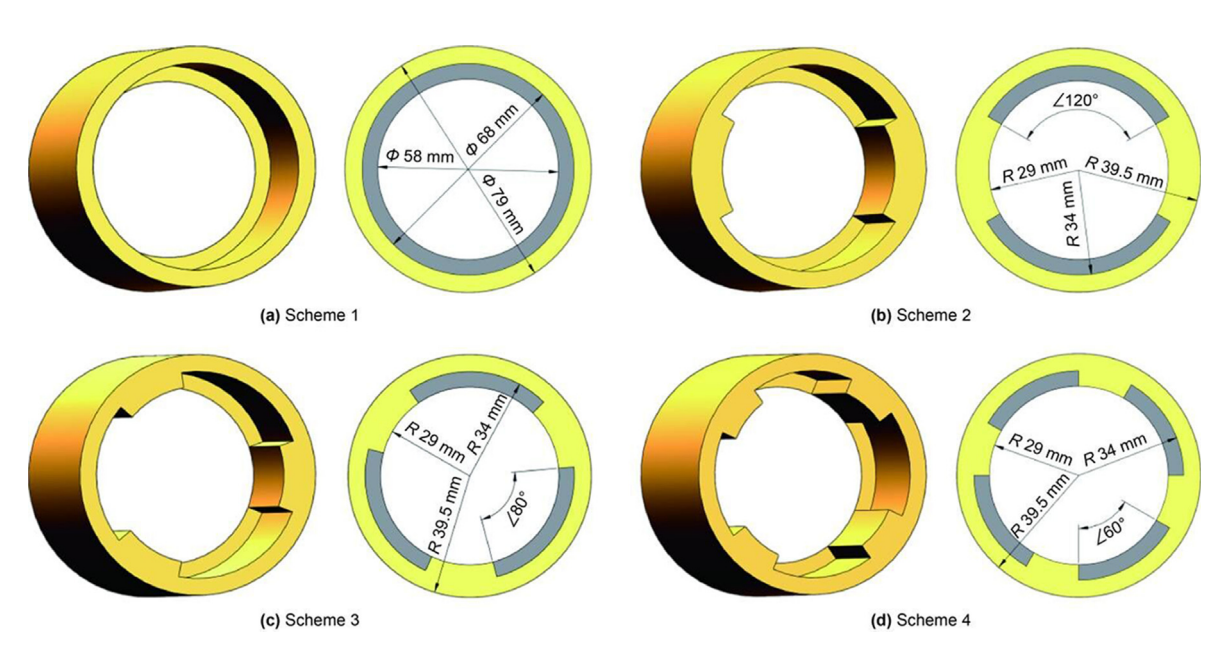


Fig. 5. Permanent magnet arrangement inside the valve seat.

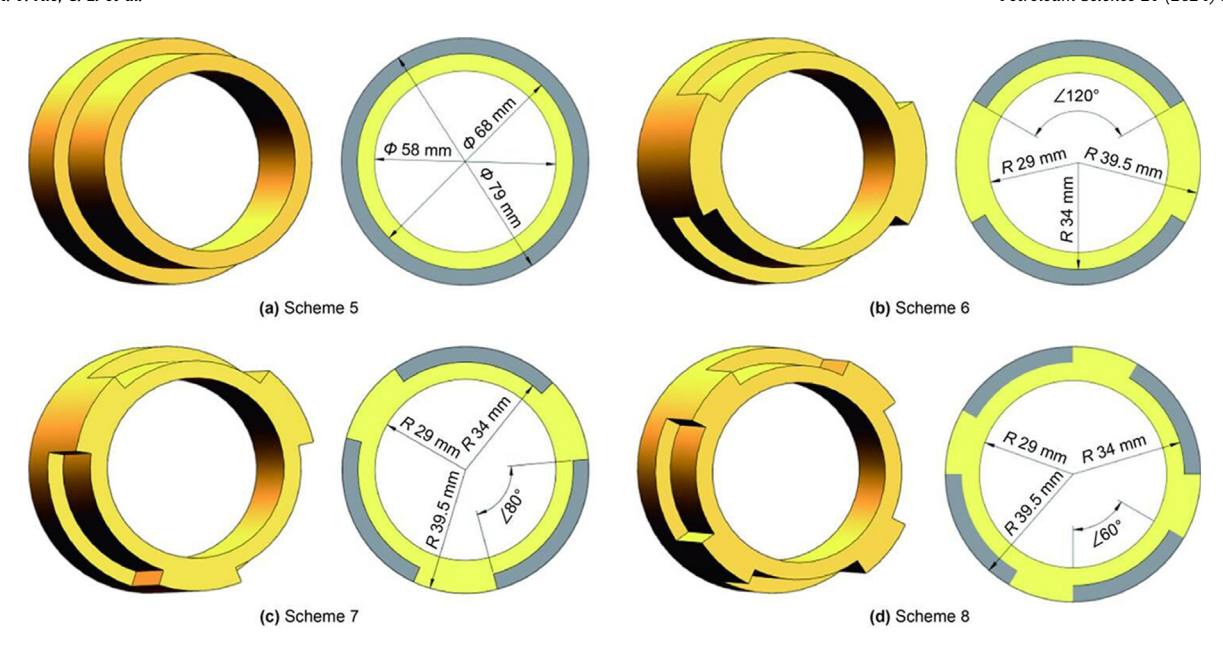
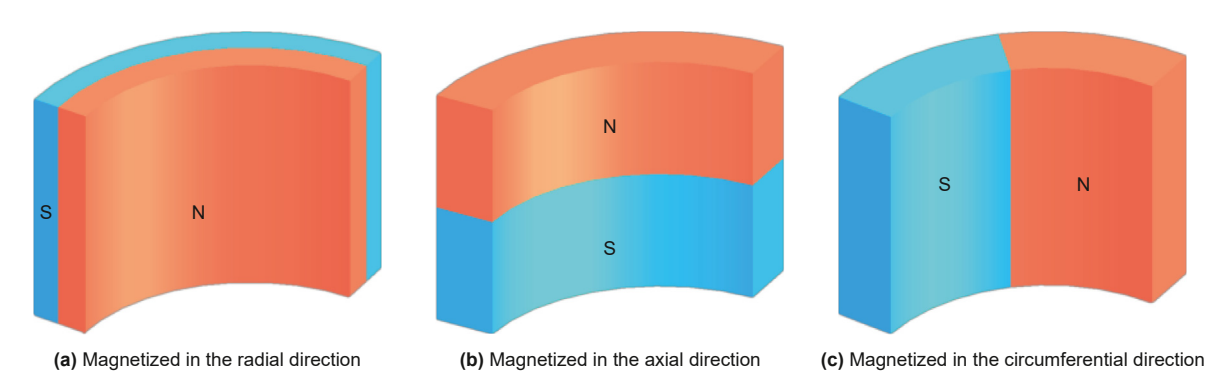


Fig. 6. Permanent magnet arrangement outside the valve seat.



 $\textbf{Fig. 7.} \ \, \textbf{Three magnetization methods of a fan-shaped permanent magnet.}$

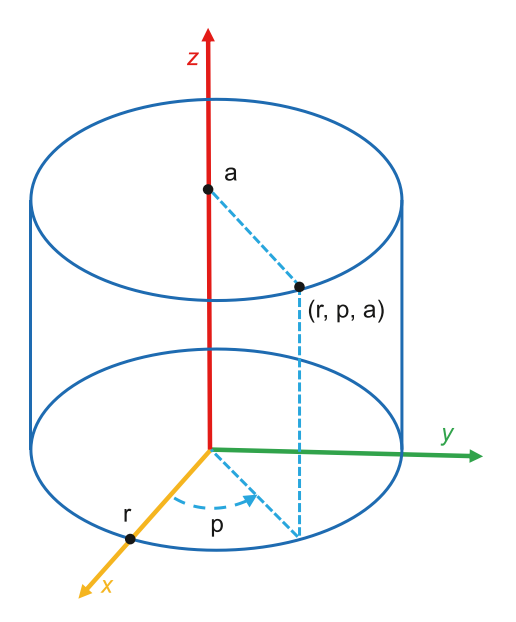


Fig. 8. The cylindrical coordinate system.

Table 1Compound magnetic field arrangement of a permanent magnet.

Number	Combined scheme	Magnetization direction		
		r	p	a
1	1r	1	0	0
2	1a	0	0	1

 Table 2

 Compound magnetic field arrangement of two permanent magnets.

Number	Combined scheme	Mag	Magnetization direction					
		r1	p1	a1	r2	p2	a2	
1	2r	1	0	0	1	0	0	
2	2p	0	1	0	0	1	0	
3	2a	0	0	1	0	0	1	
4	rp	1	0	0	0	1	0	
5	ra	1	0	0	0	0	1	
6	pa	0	1	0	0	0	1	

Table 3Compound magnetic field arrangement of three permanent magnets.

Number	Combined scheme	Ma	Magnetization direction							
		r1	p1	a1	r2	p2	a2	r3	рЗ	a3
1	3r	1	0	0	1	0	0	1	0	0
2	3p	0	1	0	0	1	0	0	1	0
3	3a	0	0	1	0	0	1	0	0	1
4	2rp	1	0	0	1	0	0	0	1	0
5	2ra	1	0	0	1	0	0	0	0	1
6	r2p	1	0	0	0	1	0	0	1	0
7	r2a	1	0	0	0	0	1	0	0	1
8	p2a	0	1	0	0	0	1	0	0	1
9	2pa	0	1	0	0	1	0	0	0	1
10	rpa	1	0	0	0	1	0	0	0	1

$$\begin{cases} \varphi_m = 0 \\ \mathbf{n} \cdot \mathbf{B} = 0 \\ \mathbf{B}_{1n} = \mathbf{B}_{2n} \\ \mathbf{H}_{1t} = \mathbf{H}_{2t} \end{cases}$$
 (1)

The magnetic field direction and size of the permanent magnet can be given by the conservation of the magnetic flux density. It includes the hypothesis equation of the magnetic field and the constitutive relation of **B**—**H**. This concept can be represented by Eq. (2).

$$\begin{cases}
\nabla \cdot \mathbf{B} = 0 \\
\mathbf{H} = -\nabla \varphi_{\text{m}} \\
\mathbf{B} = \mu_{0} \mu_{\text{r}} \mathbf{H} + \mathbf{B}_{\text{r}} \\
\mathbf{B}_{\text{r}} = \|\mathbf{B}_{\text{r}}\| \frac{\mathbf{e}}{\|\mathbf{e}\|}
\end{cases}$$
(2)

The Maxwell stress tensor method is used to solve the magnetic force on the valve cover. The calculation equation is as follows (Eq. (3)):

$$\mathbf{F}_{m} = \int_{V} \mathbf{f} dV = \int_{\partial \Omega} \left[-\frac{1}{2} \mathbf{n} (\mathbf{H} \cdot \mathbf{B}) + (\mathbf{n} \cdot \mathbf{H}) \mathbf{B}^{T} \right] dS$$
 (3)

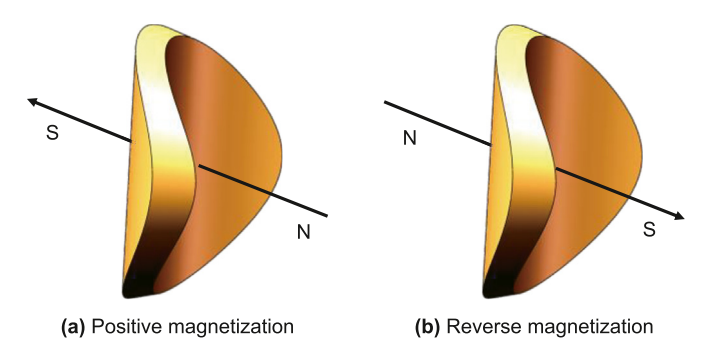


Fig. 9. Valve cover magnetization direction.

The grid size division rules of the simulation model are shown in Fig. 10.

The valve cover grid size ranged from 0.5 to 1 mm. There is a sharp corner shape between the valve seat and the permanent magnet. The grid is divided by the ultrafine scheme, and the grid size is between 0.04 and 4 mm. An automatic refinement grid is used to divide the air domain because there is an interface with the contact surface of the valve cover seat. The average unit mass of the whole model fully meets the requirements of the numerical calculation

A survey is conducted of commonly used permanent magnetic materials and metal materials in the industry to ensure that the design can be feasibly manufactured. We choose an injection-molded permanent magnet for the valve cover, cast iron for the valve seat, and N52 NdFeB for the fan-shaped permanent magnet. The magnetic field parameters for different materials in the simulation are shown in Table 5.

All the combinations of the composite magnetic field described in the previous section (Chapter 2.3) are used as the simulation scheme. The three parameters are assigned to the magnetic field direction of the permanent magnet. The magnetic field parameters of all the schemes are calculated through parametric scanning.

 Table 4

 Compound magnetic field arrangement of four permanent magnets.

Number	Combined scheme	Magne	Magnetization direction										
		r1	p1	a1	r2	p2	a2	r3	р3	a3	r4	p4	a4
1	4r	1	0	0	1	0	0	1	0	0	1	0	0
2	4p	0	1	0	0	1	0	0	1	0	0	1	0
3	4a	0	0	1	0	0	1	0	0	1	0	0	1
4	3rp	1	0	0	1	0	0	1	0	0	0	1	0
5	2r2p	1	0	0	1	0	0	0	1	0	0	1	0
6	rprp	1	0	0	0	1	0	1	0	0	0	1	0
7	r3p	1	0	0	0	1	0	0	1	0	0	1	0
8	3ra	1	0	0	1	0	0	1	0	0	0	0	1
9	2r2a	1	0	0	1	0	0	0	0	1	0	0	1
10	rara	1	0	0	0	0	1	1	0	0	0	0	1
11	r3a	1	0	0	0	0	1	0	0	1	0	0	1
12	3pa	0	1	0	0	1	0	0	1	0	0	0	1
13	2p2a	0	1	0	0	1	0	0	0	1	0	0	1
14	papa	0	1	0	0	0	1	0	1	0	0	0	1
15	p3a	0	1	0	0	0	1	0	0	1	0	0	1
16	rp2a	1	0	0	0	1	0	0	0	1	0	0	1
17	rapa	1	0	0	0	0	1	0	1	0	0	0	1
18	r2pa	1	0	0	0	1	0	0	1	0	0	0	1
19	rpap	1	0	0	0	1	0	0	0	1	0	1	0
20	2rpa	1	0	0	1	0	0	0	1	0	0	0	1
21	rpra	1	0	0	0	1	0	1	0	0	0	0	1









(a) Grid division of valve cover

(b) Grid division of valve seat

(c) Grid division of pressurepreserved controller

(d) Grid division of air domain

 $\textbf{Fig. 10.} \ \ \text{Model grid division example (Scheme 4 as an example)}.$

Table 5Magnetic field parameters of different materials.

Number	Name	Material	Magnetic parameters	
			$\mu_{\rm r}$, 1	B _r , T
1	Valve cover	Injection-molded permanent magnet	-	0.25
2	Valve seat	Cast iron	300	_
3	Fan-shaped permanent magnet	NdFeB permanent magnet	_	1.45
4	Air	Air	1.05	_

Table 6 When there is only one permanent magnet in the valve seat.

Number	Combined scheme	Magnetic force, N		
		Scheme 1	Scheme 5	
1	1r	16.86	-4.95	
2	1a	7.94	7.26	

3.2. Initial self-sealing magnetic force analysis of the pressure-preserved controller

3.2.1. Analysis of the magnetic characteristics of the valve cover during forward magnetization

When the valve cover is magnetized in the positive direction, the magnetic field direction is consistent with the force direction of the valve cover. Under different schemes, the magnetic force on the valve cover is shown in Tables 6—9.

According to Tables 6–9, when the permanent magnets are all radially (1r, 2r, 3r, 4r) magnetized, the magnetic force of the pressure-preserved controller does not exceed the gravity of the valve cover itself and is unable to achieve initial self-sealing. In addition, the magnetic force generated by the other schemes exceeds the gravity of the valve cover itself, which can achieve initial self-sealing. Comparing the magnetic force values of the eight schemes, it can be seen that when the permanent magnet is embedded inside the valve seat, the magnetic force on the valve cover as a whole presents a larger value. This shows that when the valve cover is positively magnetized, it is more reasonable for the magnetic field of the entire magnetic system to be embedded in the valve seat.

Taking the valve seat inlaid with a cylindrical permanent magnet as an example, when the permanent magnet is magnetized radially, the magnetic field of the valve cover under two inlaid

Table 7 When there are two permanent magnets in the valve seat.

Number	Combined scheme	Magnetic force, N		
		Scheme 2	Scheme 6	
1	2r	12.96	0.96	
2	2p	8.91	8.91	
3	2a	8.53	7.97	
4	гр	10.93	4.94	
5	ra	10.74	4.47	
6	pa	8.72	8.44	

Table 8When there are three permanent magnets in the valve seat.

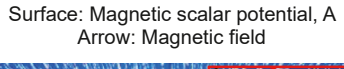
Number	Combined scheme	Magnetic force, N			
		Scheme 3	Scheme 7		
1	3r	13.05	1.52		
2	3p	8.83	8.91		
3	3a	8.46	8.03		
4	2rp	11.83	3.97		
5	2ra	11.71	3.68		
6	r2p	10.33	6.42		
7	r2a	10.08	5.84		
8	p2a	8.59	8.32		
9	2pa	8.71	8.62		
10	rpa	10.21	6.13		

modes is calculated, and the two-dimensional magnetic field distribution is obtained, as shown in Figs. 11 and 12.

Fig. 11 shows that when the permanent magnet is placed inside the valve seat, the magnetic induction line between the valve cover and the valve seat is in the same direction, forming a closed loop through the magnetic field, as shown in the red circle. At this time,

Table 9 When there are four permanent magnets in the valve seat.

Number	Combined scheme	Magnetic force	, N
		Scheme 4	Scheme 8
1	4r	12.83	2.06
2	4p	8.89	8.96
3	4a	8.54	8.13
4	3rp	11.68	3.77
5	2r2p	10.86	5.52
6	гргр	10.54	5.48
7	r3p	9.71	7.22
8	3ra	11.60	3.56
9	2r2a	10.68	5.10
10	rara	10.36	5.06
11	r3a	9.45	6.60
12	3pa	8.80	8.75
13	2p2a	8.72	8.54
14	papa	8.72	8.54
15	p3a	8.63	8.33
16	rp2a	9.54	6.80
17	rapa	9.54	6.80
18	r2pa	9.63	7.01
19	грар	9.63	7.01
20	2rpa	10.77	5.31
21	rpra	10.45	5.27



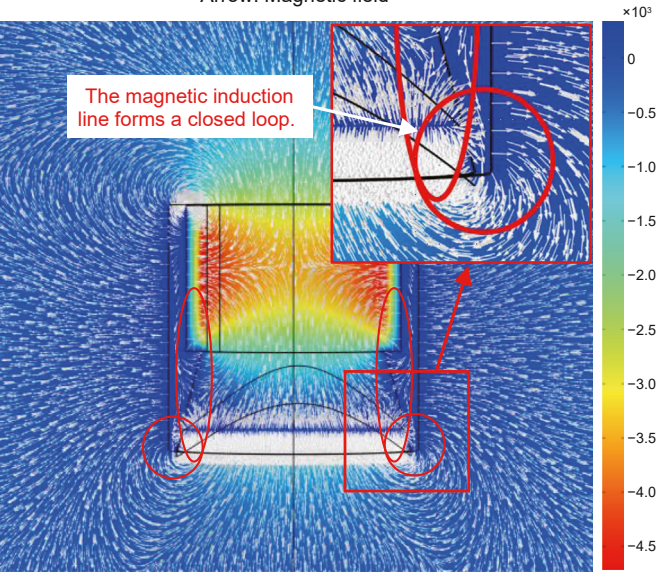


Fig. 11. Magnetic field distribution when permanent magnets are arranged inside the valve seat.

magnetic absorption occurs between the valve cover and the valve seat.

When the permanent magnet is placed outside the valve seat, there is a part of the magnetic induction line between the valve cover and the valve seat is in the opposite direction and cannot form a through magnetic field, as shown in the white circle in Fig. 12.

In this case, there is a repulsive magnetic field between the valve cover and the valve seat. When the total magnetic field cannot offset this part of the repulsive magnetic field, the magnetic system shows a repulsive force. Through the above analysis, the reason why the magnetic force is greater when the permanent magnet is placed inside the valve seat when the valve cover is positively magnetized is clarified.

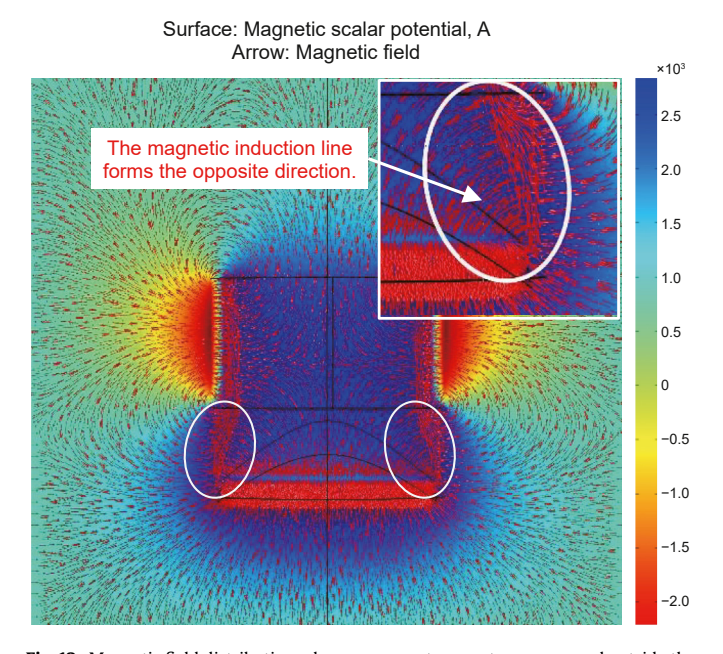


Fig. 12. Magnetic field distribution when permanent magnets are arranged outside the valve seat.

The magnetic force on the valve cover is sorted, as shown in Fig. 13.

According to the figure, when the number of permanent magnets in the valve seat is the same, the more permanent magnets there are in the radial magnetization (r direction), the greater the magnetic force on the valve cover. The influence of the magnetization direction of the permanent magnet in the valve seat on the magnetic force of the valve cover is in the order of radial > axial > circumferential. This shows that the radial magnetic field is the main magnetic field of the self-sealing scheme of the pressure-preserved controller. At the same time, when the magnetic field direction of all the permanent magnets inlaid in the valve seat is radial, comparing the relationship between the number of different inlays and the magnetic force, it is found that the magnetic force is greater when one permanent magnet is inlaid inside the valve seat. At the same time, when the magnetic field direction of all permanent magnets inside the valve seat is radial, comparing the relationship between different schemes and magnetic force, it is found that the magnetic force is greater when the permanent magnet inside the valve seat is a cylinder. This is because when the permanent magnet is a cylinder, it occupies more space, and its own magnetic field is stronger. For other schemes, the radial volume of the permanent magnet is basically the same, so the magnetic force of the valve cover under the action of the three is basically the same, so it can be flexibly selected.

3.2.2. Analysis of the magnetic characteristics of the valve cover during reverse magnetization

When the valve cover is reversely magnetized, the magnetic field direction is opposite to the force direction of the valve cover. Under different schemes, the magnetic force on the valve cover is shown in Tables 10–13.

According to the above tables, except for the scheme of a cylindrical permanent magnet arranged inside the valve seat, the magnetic force generated by other schemes can achieve initial self-sealing. It can be seen from the data in the comparison table that when the permanent magnet is arranged outside the valve seat, the magnetic force on the valve cover is greater. This shows that when

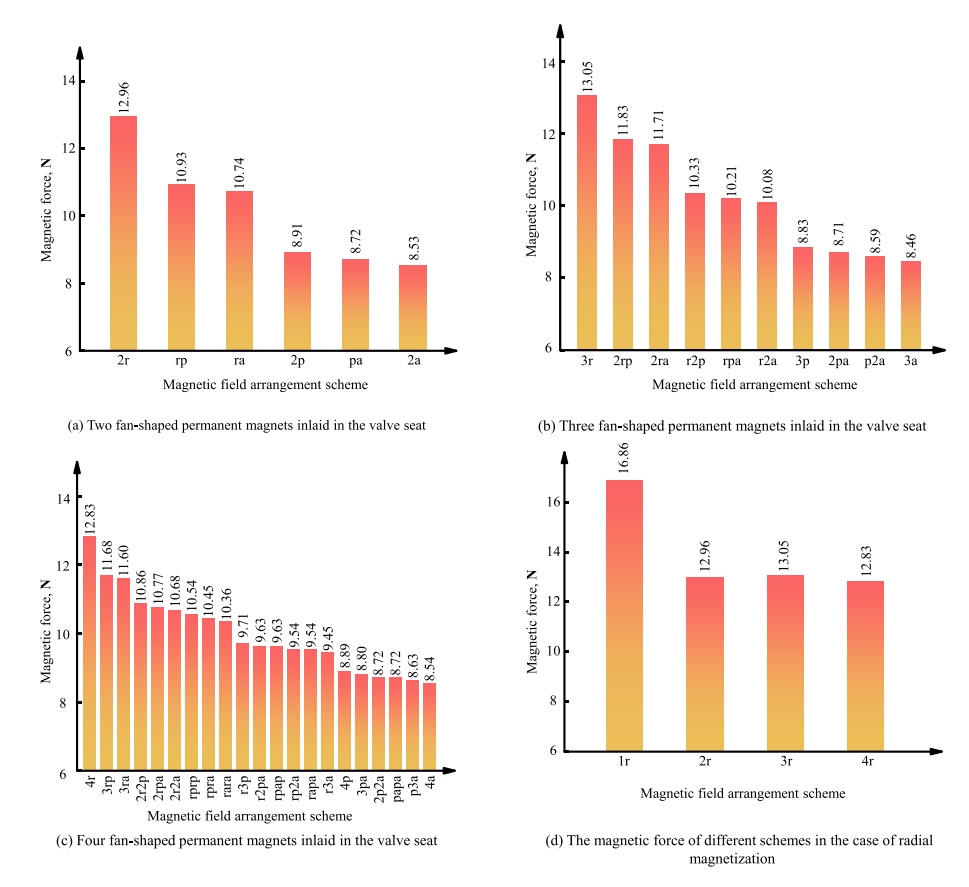


Fig. 13. Magnetic force comparison of different magnetic field arrangement schemes.

Table 10When there is one permanent magnet in the valve seat (reverse magnetization).

Number	Combined scheme	Magnetic force, N	
		Scheme 1	Scheme 5
1	1r	0.72	22.47
2	1a	9.35	10.51

Table 11When there are two permanent magnets in the valve seat (reverse magnetization).

Number	Combined scheme	Magnetic force, N		
		Scheme 2	Scheme 6	
1	2r	4.92	16.78	
2	2p	8.91	8.91	
3	2a	9.30	9.84	
4	rp	6.91	12.85	
5	ra	7.11	13.32	
6	pa	9.11	9.38	

the valve cover is reversely magnetized, the magnetic field distribution of the whole magnetic system is more reasonable outside the valve seat. At the same time, under these conditions, the permanent magnet adopts radial magnetization, and the effect of the composite magnetic field is also the best.

The two-dimensional magnetic field distribution of the pressure-preserved controller under two operating conditions is shown in Figs. 14 and 15. Comparing the two diagrams, when the permanent magnet is arranged inside the valve seat, there is a magnetic induction line in the opposite direction on the outer

 $\begin{tabular}{ll} \textbf{Table 12} \\ \textbf{When there are three permanent magnets in the valve seat (reverse magnetization)}. \\ \end{tabular}$

Number	Combined scheme	Magnetic force, N	
		Scheme 3	Scheme 7
1	3r	4.69	16.24
2	3p	8.83	8.91
3	3a	9.20	9.79
4	2rp	5.88	13.81
5	2ra	6.00	14.11
6	r2p	7.35	11.39
7	r2a	7.60	11.97
8	p2a	9.08	9.50
9	2pa	8.95	9.20
10	rpa	7.48	11.68

surface of the valve cover (the transverse red coil in Fig. 14), and the magnetic induction line of the valve cover itself extends to the permanent magnet to produce a penetrating magnetic induction line. The reverse magnetic field on the upper surface causes the valve cover to produce an upward repulsive force, and the magnetic field of the valve cover itself results in upward suction, which comprehensively produces the magnetic force that presses the valve cover. There is a magnetic induction line in the opposite direction near the surface of the valve cover and the valve seat to hinder the pressing of the valve cover so that the valve cover produces a downward repulsion. Moreover, the total magnetic force decreases.

When the permanent magnet is arranged outside the valve seat, four annular magnetic circuits (shown in the white coil in Fig. 15) are generated on the valve cover, forming multiple magnetic fields,

Table 13When there are four permanent magnets in the valve seat (reverse magnetization).

Number	Combined scheme	Magnetic force, N	
		Scheme 4	Scheme 8
1	4r	5.03	15.80
2	4p	8.89	8.96
3	4a	9.24	9.79
4	3гр	6.14	14.11
5	2r2p	6.95	12.39
6	rprp	7.26	12.42
7	r3p	8.07	10.69
8	3ra	6.23	14.32
9	2r2a	7.13	12.80
10	rara	7.43	12.84
11	r3a	8.33	11.32
12	3pa	8.98	9.17
13	2p2a	9.07	9.38
14	papa	9.07	9.38
15	p3a	9.15	9.58
16	rp2a	8.25	11.11
17	rapa	8.25	11.11
18	r2pa	8.16	10.90
19	грар	8.16	10.90
20	2rpa	7.04	12.59
21	rpra	7.34	12.63

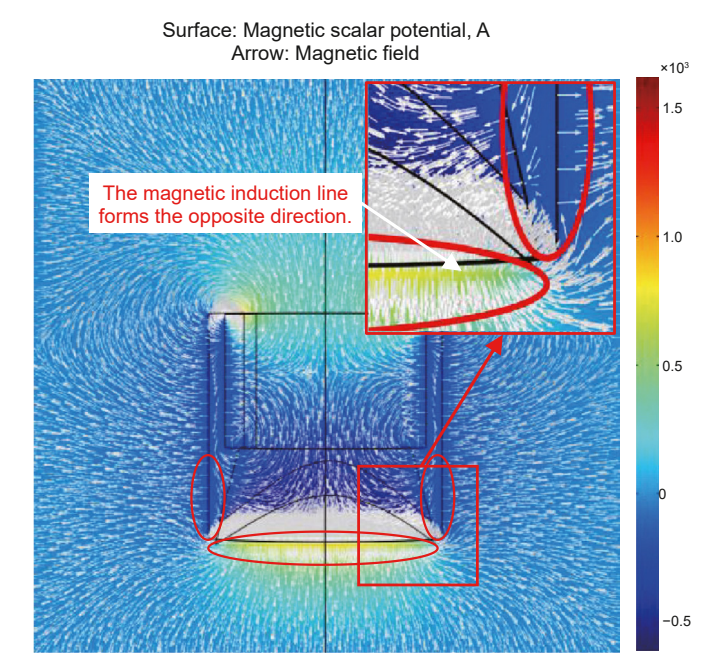


Fig. 14. Magnetic field distribution when permanent magnets are arranged inside the valve seat.

which make the valve cover tightly attracted. The above analysis illustrates why the magnetic force is greater when the permanent magnet is arranged outside the valve seat when the valve cover is reversely magnetized.

Finally, according to Table 10–13, the same magnetic comparison diagram as above can be obtained. It can also be determined that the radial magnetization effect of the permanent magnet is the best, so it is no longer described in detail here.

3.3. Results and comparisons

By comparison, the permanent magnet should be arranged inside the valve seat when the valve cover is forward magnetizing.

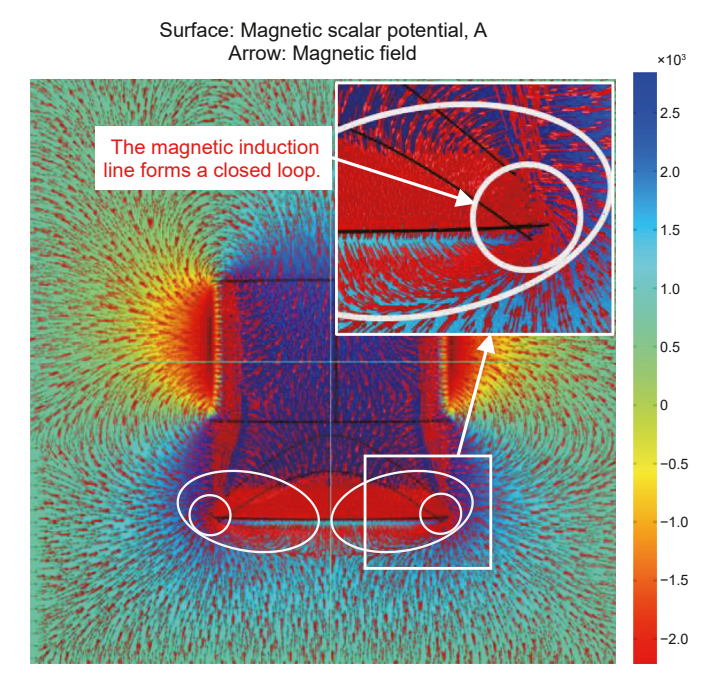


Fig. 15. Magnetic field distribution when permanent magnets are arranged outside the valve seat.

When the valve cover is reversely magnetized, the permanent magnet should be arranged outside the valve seat. The magnetic force that occurs when the magnetization direction of the permanent magnet on the valve seat is radial is shown in Fig. 16. It can be seen in the figure that under the above conditions, the magnetic force on the valve cover can reach 12.83–22.47 N, far exceeding the gravity of the valve cover itself. At this time, the valve cover can be closed at any angle to achieve initial self-sealing through magnetic attraction; thus, the radial magnetization of the permanent magnet on the valve seat is considered the optimal magnetic circuit design.

Considering that the outside of the valve seat needs to contact the inner diameter of the corer, the scheme of the permanent magnet arranged inside the valve seat is preferred to prevent damage to the permanent magnet during the installation process. At the same time, considering that the processing of cylindrical permanent magnets (Scheme 1) is difficult, multiple permanent tile magnets should be preferably embedded in the valve seat. In summary, Scheme 3 is selected as the final optimization scheme, and its initial pre-tensioning force is 13.05 N.

4. Verification and discussion

4.1. Initial self-sealing verification

4.1.1. Test preparation

At present, there is little research on magnetically controlled self-sealing pressure-preserved coring, and there is no relevant test platform for reference in the research and development process. In response, a sealing performance test platform was independently developed, as shown in Fig. 17.

According to the simulation optimization scheme, three 90° tile permanent magnets (N52 NdFeB magnets) are chosen for installation in the valve seat, as shown in Fig. 18.

The pressure-preserved controller was mounted on the test platform and debugged to ensure that there were no problems, as shown in Fig. 19.

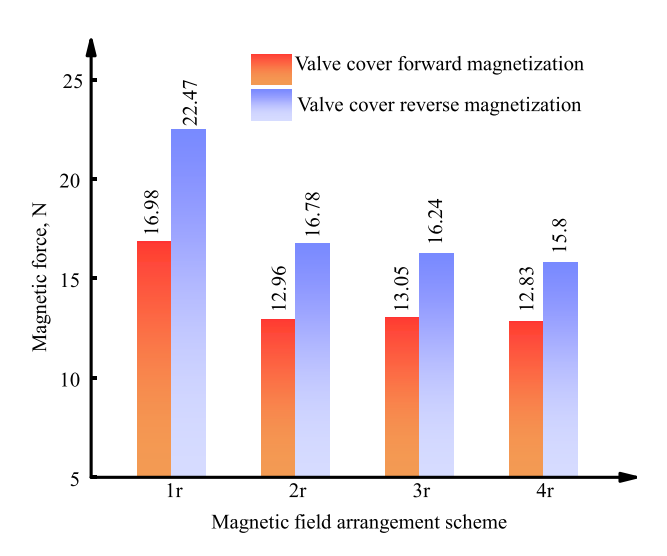


Fig. 16. Comparison of magnetic forces when the permanent magnet on the valve seat is magnetized radially.

4.1.2. Testing method

To verify the correctness of the magnetically controlled self-sealing theory, experimental validations were conducted on multiple composite magnetic fields, as shown in Scheme 3 (Table 8). Permanent magnets with axial magnetization, radial magnetization and circumferential magnetization were processed, as shown in Fig. 20. The initial pre-tensioning force of the pressure-preserved controller was measured by a dynamometer, as shown in Fig. 21.

The pressure-preserved controller is installed in the sealing performance test platform. The test platform is then placed horizontally. Under these conditions, the initial self-sealing of the valve cover is unaffected by gravity and solely influenced by magnetic force. The measurement probe of the f dynamometer is inserted through the valve seat, aligning perpendicularly to the center of the valve cover. The force recorded by the advancing gauge represents the initial pre-tensioning force of the pressure-preserved controller. To minimize measurement errors, five sets of measurements were conducted for each composite magnetic field.

When using the test platform to detect the initial self-sealing effect of the pressure-preserved controller, two mutually verified testing methods were designed as follows.

(1) When the valve cover is closed, the transparent pressurepreserved cabin is filled with air through the blue trachea (Fig. 19(d)). A pressure range of 0.2–0.5 MPa was used and



Fig. 18. Magnetically controlled self-sealing pressure-preserved controller.

maintained for 1 min after the gas source was removed. The internal pressure of the cabin is monitored by a pressure sensor to observe whether the sensor parameters change. For the sake of insurance, the monitoring time is set to 30 min. If there is no pressure drop, it is proven that the initial self-sealing can be achieved.

(2) In the multiangle test, lubricating oil is poured into the valve seat cavity (as shown in Fig. 22). We observe whether there are bubbles. If there is no bubble, the initial self-sealing performance of the magnetically controlled self-sealing pressure-preserved controller is good, which is mutually verified with the method in (1).

4.1.3. Initial self-sealing test results

The experimental results of the initial pre-tensioning force were averaged and compared with the numerical simulation results, as shown in Fig. 23. The test results are largely consistent with the simulation calculations. This consistency substantiates the accuracy of the simulation results and supports the validity of the magnetically controlled self-sealing theory. Furthermore, the optimally selected radial composite magnetic field (3r) generated a magnetic force of 13.34 N, significantly exceeding the gravity of the valve cover of 2.8 N. This demonstrates the feasibility of the magnetically controlled self-sealing technology approach.

To verify the accuracy of the test, four pressure gradients of 0.2, 0.3, 0.4, and 0.5 MPa were used as the test control groups. Each group was observed for 30 min, and every 2 h there was a sealed cycle test. The sealing curve is shown in Fig. 24.

The four groups of curves in the figure are gentle, and there is no

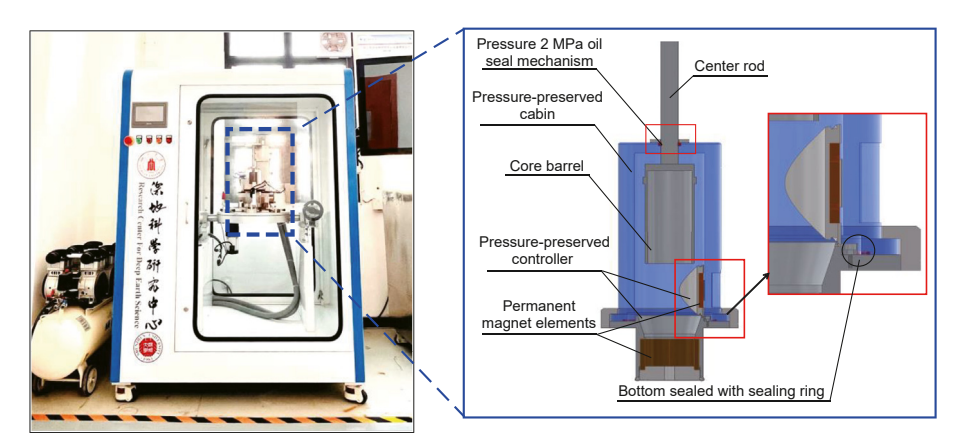


Fig. 17. Sealing performance test platform.



Fig. 19. Debugging of the pressure-preserved controller on the sealing test platform.

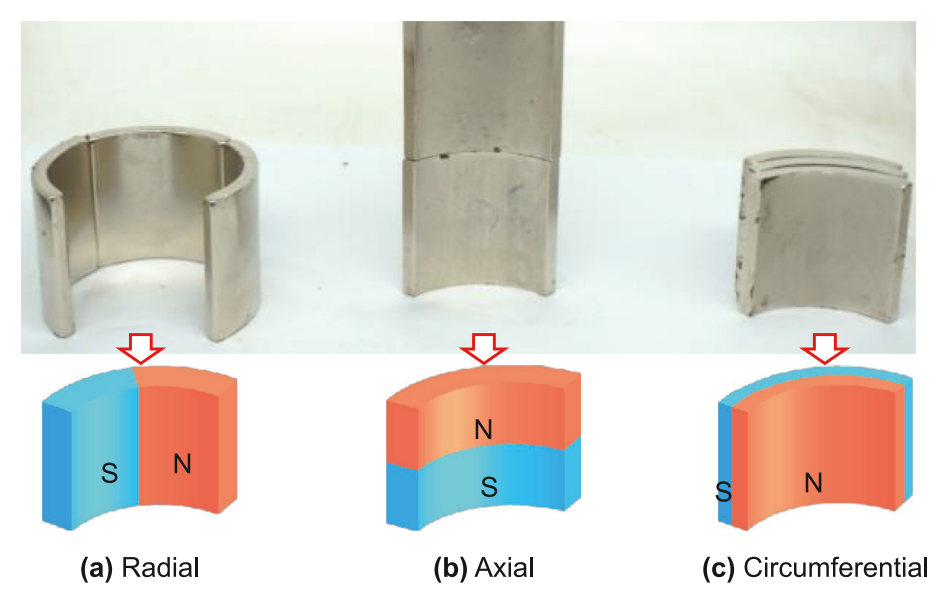


Fig. 20. Fabricated permanent magnets.

pressure drop, indicating excellent sealing. Afterward, the lubricating oil was added inside the valve seat, and no small bubbles were generated (as shown in Fig. 25), indicating that there was no leakage.

In summary, the sealing performance of the magnetically controlled self-sealing scheme was verified through two testing methods, proving that the preferred magnetically controlled scheme has excellent applicability and achievability. Furthermore, it has achieved initial success at the theoretical and experimental levels.

4.2. Industrial test of magnetically controlled self-sealing pressurepreserved coring technology

In view of the above scheme, a magnetically controlled self-sealing pressure-preserved coring device for coalbed methane was preliminarily designed, as shown in Fig. 26. The main purpose of the device is to obtain in situ gas pressure. Therefore, the pressure-preserved capacity should be greater than the pressure of the in situ gas content. Typically, the in situ gas pressure does not exceed 2 MPa, and even in gas outbursts, the in situ gas content is

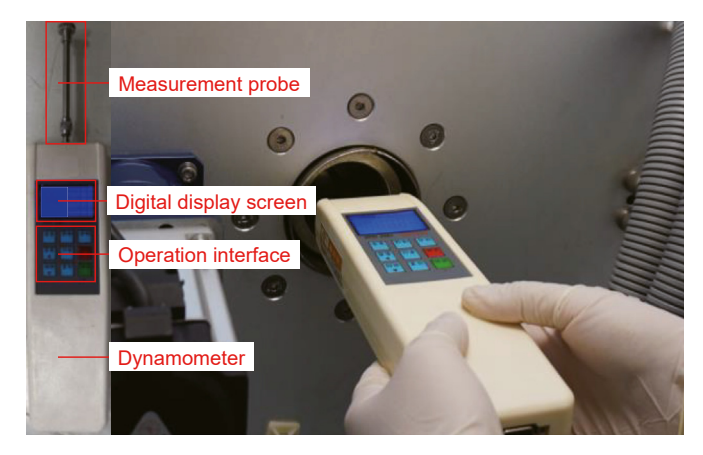


Fig. 21. Testing method of initial pre-tensioning force.

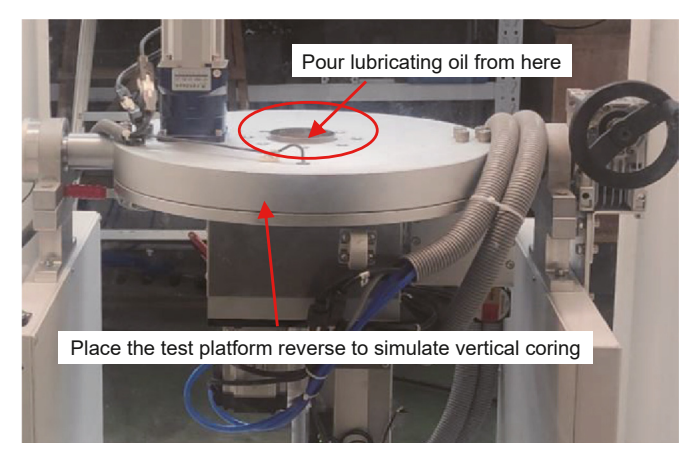


Fig. 22. An inverted pressure-preserved controller was used to verify the initial sealing performance.

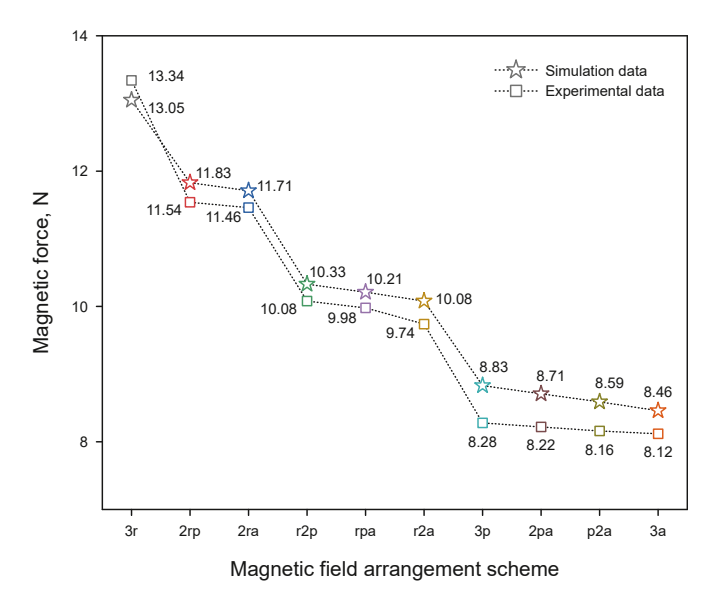


Fig. 23. Initial pre-tensioning force of the pressure-preserved controller under different composite magnetic fields.

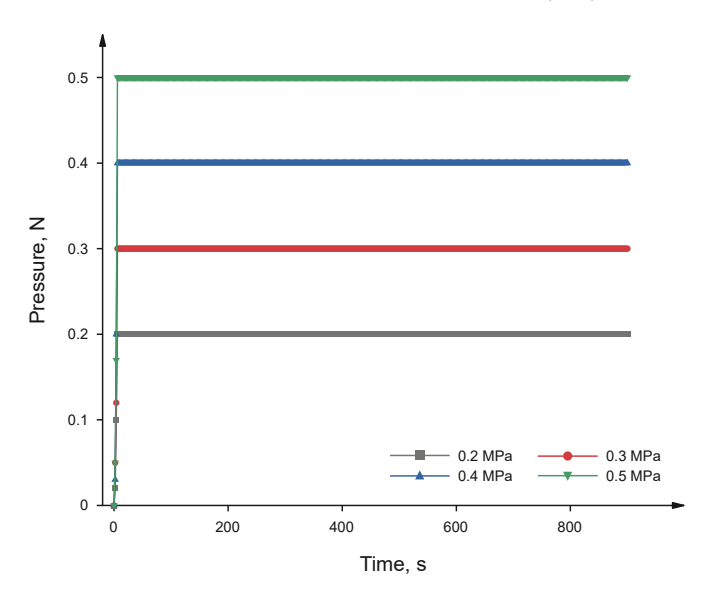


Fig. 24. Sealing curve.

within 3 MPa (Yao et al., 2016; Hou et al., 2021; Tu et al., 2021; Wang H. et al., 2021). Therefore, to safely obtain in situ gas, the rated working pressure was set to 8 MPa. Importantly, this value does not indicate the ultimate compressive strength of the pressure-preserved controller but rather its ability to function reliably over an extended period at 8 MPa.

To further substantiate the feasibility of magnetically controlled self-sealing pressure-preserved coring technology, pressure-preserved coring tests were conducted 50 m underground at the experimental site.

As shown in Fig. 27, following the coring process, successful closure of the pressure-preserved controller was observed (Fig. 27(c)). When the pressure tap of the pressure-preserved coring device is opened, there is a water column injection (Fig. 27(d)). These experimental results demonstrate that the pressure-preserved controller can effectively achieve magnetically controlled self-sealing, demonstrating its robust pressure-preserved properties. Moreover, this test thoroughly validates the feasibility of magnetically controlled self-sealing for engineering applications.

4.3. The target reservoir parameters of magnetically controlled selfsealing pressure-preserved coring

The performance of NdFeB permanent magnets is affected by factors such as reservoir temperature, pH, fluid media, and dynamic loads. To address this issue, industrial practices often involve protective treatments, primarily through coating. The coating enhances the temperature resistance and corrosion resistance of permanent magnets. Based on this, a detailed analysis of the reservoir parameters was conducted.

4.3.1. Target reservoir temperature

To ensure the reliability of magnetically controlled self-sealing pressure-preserved coring technology through stronger magnetic forces in the composite magnetic field, N52 NdFeB permanent magnets with maximum remanence were initially selected. The impact of temperature on magnetically controlled self-sealing pressure-preserved coring technology is primarily manifested in

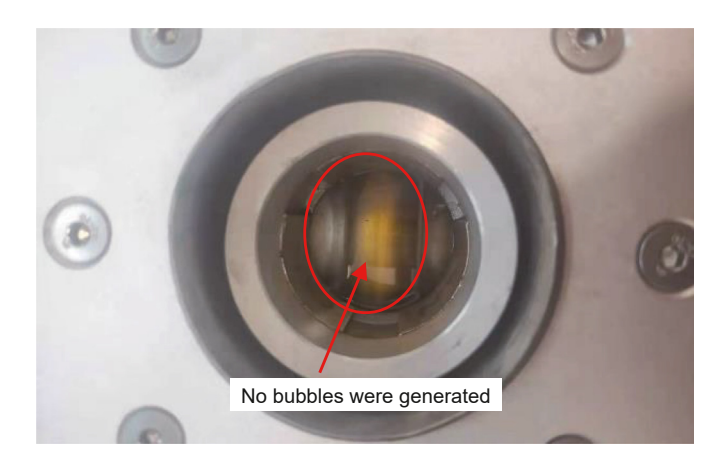


Fig. 25. No bubbles were generated in the injected lubricating oil.



Fig. 26. Pressure strength test of the pressure-preserved controller.

the temperature resistance performance of the materials. The pressure-preserved controller includes two types of permanent magnet materials and one metal material. The maximum working temperatures of materials available in the industry have been studied. The working temperatures for metal materials $(400-500\,^{\circ}\text{C})$ and injection-molded permanent magnets $(<150\,^{\circ}\text{C})$ are higher than that of N52 NdFeB permanent magnets $(80\,^{\circ}\text{C})$. Consequently, the target reservoir temperature is $80\,^{\circ}\text{C}$.

4.3.2. Target reservoir pressure

Reservoir pressure and temperature are primarily influenced by factors such as underground depth, geological structures, and geothermal gradients, which typically increase with depth (Buijze et al., 2023; Buscheck et al., 2024). When the target reservoir

temperature is 80 °C, using the geothermal gradient to estimate the target reservoir pressure is an efficient method (Thomas et al., 2020). The average geothermal gradient for geological formations is approximately 3–5 °C per 100 m of depth (Pasquale et al., 2014; Chu et al., 2021; Hu et al., 2023). With an average surface temperature of 15 °C, a reservoir temperature of 80 °C corresponds to a depth of approximately 1625 m. The reservoir pressure P increases with depth, and its empirical formula is as follows:

$$P = \rho \times g \times h \tag{4}$$

The ρ typically ranges from 1700 to 2000 kg/m³. For this calculation, a commonly used value of 1850 kg/m³ is chosen (Guo et al., 2023b);

Under these conditions, using Eq. (4), the reservoir pressure is calculated to be 29.5 MPa. Therefore, we set the target reservoir pressure at 30 MPa.

To verify the pressure-bearing capacity of the pressurepreserved controller under dynamic loading, combined with the actual application point of view, a strength check was carried out through a dynamic load test after pressure-preserved coring.

First, the bailout core is extracted according to Section 4.2. After coring, the device was transported to a safe area. The pressure-preserved controller had already achieved self-sealing. The coring device was then dynamically pressurized using a pressure pump for a pressure-bearing performance test, as shown in Fig. 28.

Eight pressure gradients were used: 0, 2, 4, 6, 8, 10, 20, and 30 MPa. The load was increased to the next gradient every half hour. To verify the long-term pressure-preserved capability of the magnetically controlled self-sealing pressure-preserved controller under real conditions, extended pressure-preserved tests were conducted at 8 and 30 MPa. These tests aimed to evaluate the controller's sustained pressure-bearing capacity in both pressure-preserved coring for coalbed methane and in target reservoir pressure environments.

The results of the pressure-bearing performance test are shown in Fig. 29.

The data indicate that in the pressure-preserved coring device designed for coalbed methane extraction, the system successfully maintained pressure for 7.5 h without any pressure drop. This finding underscores the significant application value of magnetically controlled self-sealing pressure-preserved coring technology in such scenarios. Additionally, under a target reservoir pressure of 30 MPa, the device consistently sustained pressure for 7.5 h, confirming the robust pressure-bearing capability of the magnetically controlled self-sealing pressure-preserved controller in such high-pressure environments.



(a) Drilling derrick



(b) Coring



(c) The pressure-preserved controller is closed



(d) Successful sealing

Fig. 27. Pressure-preserved coring tests were performed 50 m underground at the experimental site.



Fig. 28. Pressure-bearing performance test of the pressure-preserved coring device.

4.3.3. pH

The NdFeB permanent magnets that were selected were coated with a triple layer of nickel-copper-nickel (Ni-Cu-Ni). This coating enhances corrosion resistance, particularly in specific chemical environments. It typically resists oxidation, making it suitable for use in acidic and alkaline environments. Therefore, maintaining the integrity of the magnet coating as much as possible below the working temperature ensures that its magnetic properties are not diminished. Accordingly, the pH range for commercially used permanent magnets has been investigated, and it was preliminarily determined that NdFeB permanent magnets are generally used within a pH range of 4–9. They exhibit good corrosion resistance in neutral and mildly acidic environments (pH 6 to 7) as well as in mildly alkaline environments (pH 8 to 9). However, under more extreme acidic (pH < 4) or alkaline (pH > 9) conditions, the nickel coating may corrode. Therefore, this study tested the integrity of the coating and the surface magnetic strength at pH values ranging from 1 to 4 and from 9 to 14 to verify the corrosion resistance of the magnets in various pH environments. The specifics are as follows:

First, in the laboratory with pH values ranging from 1 to 4 and from 9 to 14 standard solutions, ten permanent magnet samples with uniform coatings were selected. Before the commencement of the experiment, a Gauss meter was used to measure the surface magnetism of the permanent magnet samples, and the results are displayed in Fig. 30. It is evident from the data that the surface magnetic strength of the magnet samples generally remained within the range of 1400–1500 Gauss.

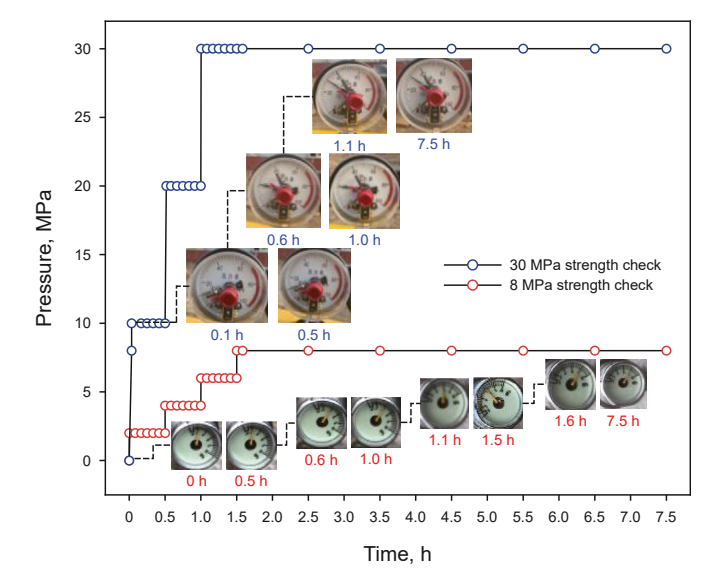


Fig. 29. The results of the pressure-bearing performance test.

The permanent magnet samples were sequentially immersed in solutions of varying pH values according to their assigned numbers, as depicted in Fig. 31. Based on field experience, the duration of each pressure-preserved coring working was approximately 8 h. After 6 cycles of coring, the surface of the permanent magnet was examined, and the soaking time was 48 h. Subsequently, a second measurement of their surface magnetism was taken. Additionally, the coating of each sample was observed for any reactions with the pH solutions and checked for signs of corrosion.

After soaking the permanent magnet sample for 48 h, ten sample surfaces did not show any signs of corrosion. The surface magnetism of the sample before and after soaking was compared, as shown in Fig. 32.

The surface magnetism of the permanent magnets of the ten samples is basically stable and is not affected by the pH. After coating treatment, the material can have long-term stable magnetic properties and exhibit good corrosion resistance in a liquid environment with a pH range of 1–14.

In summary, the permanent magnets selected in this study exhibit good corrosion resistance and magnetic properties in the pH range of 1–14 and can be used in high acid value reservoirs.

4.3.4. Fluid media

To assess the magnetic properties of permanent magnets in complex fluid environments, the most common test, apart from evaluating the magnetic properties of permanent magnets in various pH fluid media, is the salt spray test. This long-duration experiment is used to verify the corrosion resistance of permanent magnets in complex fluid media (Qin and He, 2013; Xi et al., 2020; Gao Y.M. et al., 2021; Yang et al., 2023). Many studies (Isotahdon et al., 2014, 2015; Högberg et al., 2016; Li et al., 2017; Dos Santos and Panossian, 2019; Chowdhury et al., 2021) have thoroughly confirmed that nickel-plated magnets, particularly those with a Ni—Cu—Ni coating, exhibit excellent corrosion resistance in salt spray tests, with the coating proving effective even after 600 h of exposure (Högberg et al., 2016). Therefore, it can be concluded that permanent magnets will demonstrate robust corrosion resistance in fluid media.

Moreover, during the initial design phase, the impact of drilling fluid invasion and its potential effect on the performance of the pressure-preserved controller were thoroughly considered. To address this issue, our team developed an innovative drilling fluid channel design, ensuring that the drilling fluid does not flow through the pressure-preserved controller. In subsequent research, we will continually consider the potential impact of complex environmental factors such as drilling fluids, if they flow extensively through the pressure-preserved controller, on the magnetically controlled self-sealing performance. This will enhance the stability of the technology in complex environments.

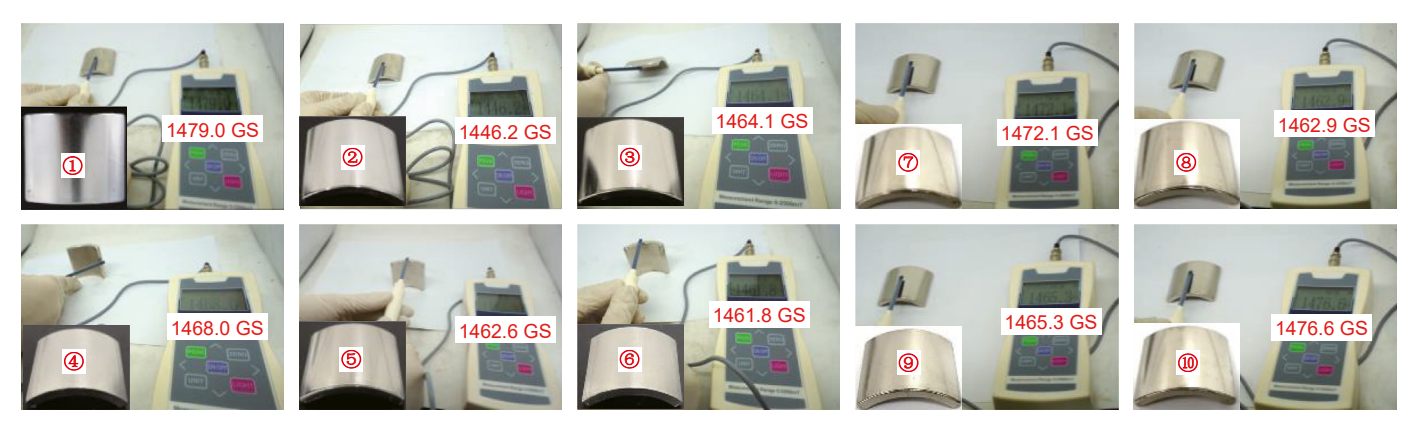
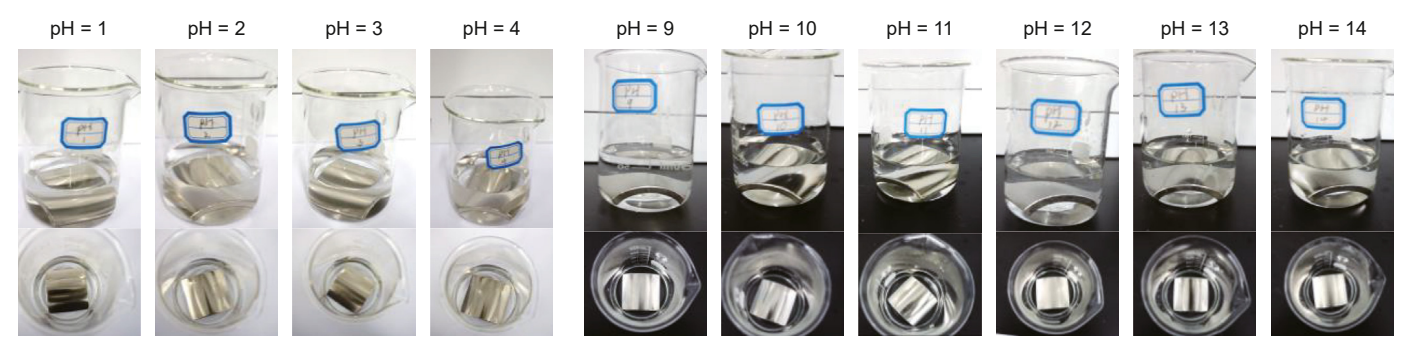


Fig. 30. Surface magnetism of the permanent magnet samples.



(a) The samples were soaked in acidic solution

(b) The samples were soaked in alkaline solution

Fig. 31. Permanent magnet samples were immersed in different pH solutions according to the number.

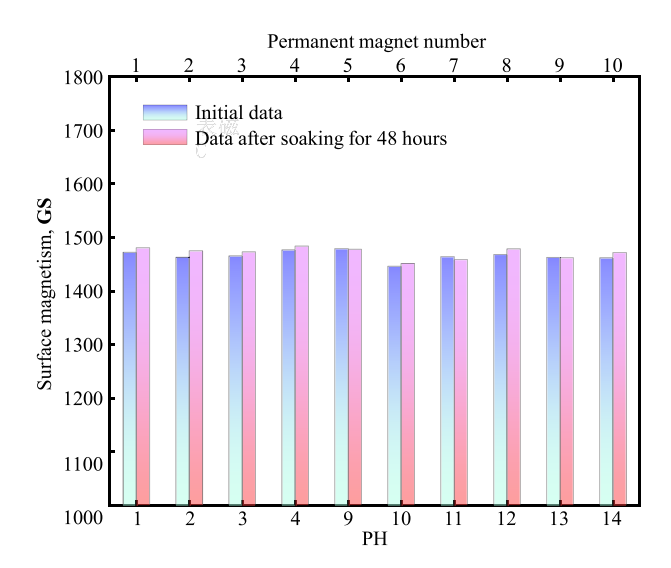


Fig. 32. Comparison of the surface magnetism of permanent magnet samples before and after soaking.

5. Conclusions

To address self-sealing performance defects in flap valves, an innovative magnetically controlled self-sealing pressure-preserved controller has been designed. Through magnetic force, noncontact self-sealing of the pressure-preserved controller in any direction is realized, and the fault tolerance rate of the initial seal of the pressure-preserved process increases. It is proven that this

technology can be applied to deep earth resource pressurepreserved exploration through scheme design, simulation calculations, test verification, and industrial testing. The magnetically controlled self-sealing pressure-preserved coring technology could be applied to natural gas, coalbed methane, natural gas hydrate, oil, and other engineering fields. The research results provide technical support for multidirectional pressure-preserved coring and thus a new technical route for deep energy exploration by coring. The main achievements and conclusions can be summarized as follows.

- (1) The magnetically controlled self-sealing pressure-preserved coring technique is proposed for the first time. This process involves noncontact self-sealing by magnetic force, which preserves the structure of the pressure-preserved coring device and improves its fault tolerance. It has the ability to preserve horizontal and inclined pressure, which provides technical support for the technical problems of horizontal pressure-preserved coring in petroleum and other fields.
- (2) By analyzing the magnetic force, the influence of the magnetization direction of the permanent magnet integrated on the valve seat on the magnetic force of the valve cover from large to small is radial > axial > circumferential. The radial magnetic field is the optimal magnetic field in the magnetically controlled scheme. The initial pre-tensioning force of the optimal magnetic field is 13.05 N.
- (3) A sealing test platform was developed to test the initial self-sealing performance of the magnetically controlled self-sealing pressure-preserved controller. The test results indicate that the pressure-preserved controller is capable of sustaining initial self-sealing over extended periods in

- multiple directions under gas pressures ranging from 0.2 to 0.5 MPa. Furthermore, the accuracy of the simulation results was verified by the test platform and dynamometer, and the validity of the magnetically controlled self-sealing theory was corroborated. The initial pre-tensioning force of the actual scheme reaches 13.34 N.
- (4) A magnetically controlled self-triggered pressure-preserved coring device tailored for coalbed methane was designed, and pressure-preserved coring was carried out to verify the feasibility of industrial applications of the technology. Moreover, through dynamic pressure gradient tests after coring, it was verified that the device can realize stable selfsealing and pressure-preserved under pressure environments of 2, 4, 6, 8, 10, 20 and 30 MPa. This proves the reliability of magnetically controlled self-sealing pressurepreserved coring technology and provides a technical basis for the innovative design of pressure-preserved controllers.
- (5) Through comprehensive theoretical analysis and experimental validation, the technology has been demonstrated to withstand extreme reservoir conditions, including temperatures up to 80 °C, pressures up to 30 MPa, and compatibility with a pH range of 1–14. Consequently, it is apt for the multifaceted environments encountered in downhole drilling fluids.

CRediT authorship contribution statement

Gui-Kang Liu: Writing — original draft, Validation, Software, Methodology, Investigation, Conceptualization. **He-Ping Xie:** Writing — review & editing, Supervision, Resources, Project administration, Funding acquisition. **Cong Li:** Writing — review & editing, Visualization, Project administration, Investigation, Formal analysis. **Zhen-Xi You:** Software, Investigation, Formal analysis. **Xiao-Jun Shi:** Visualization, Software, Investigation. **Jian-Jun Hu:** Visualization, Software, Formal analysis, Conceptualization. **Ming-Zhong Gao:** Supervision, Resources, Data curation.

Declaration of competing interest

The authors declare that they have no known competing financial interests or personal relationships that could have appeared to influence the work reported in this paper.

Acknowledgments

This research was supported by the National Natural Science Foundation of China (52225403, 52304146), the Sichuan Science and Technology Program (2023NSFSC0919, 2023NSFSC0790) and the China Postdoctoral Science Foundation (2023M742460).

References

- Abegg, F., Hohnberg, H.J., Pape, T., et al., 2008. Development and application of pressure-core-sampling systems for the investigation of gas-and gas-hydratebearing sediments. Deep Sea Res. Oceanogr. Res. Pap. 55 (11), 1590–1599. https://doi.org/10.1016/j.dsr.2008.06.006.
- Buijze, L., Veldkamp, H., Wassing, B., 2023. Comparison of hydrocarbon and geothermal energy production in The Netherlands: reservoir characteristics, pressure and temperature changes, and implications for fault reactivation. Neth. J. Geosci. 102, e7. https://doi.org/10.1017/njg.2023.6.
- Buscheck, T.A., Goodman, A., Lackey, G., et al., 2024. Underground storage of hydrogen and hydrogen/methane mixtures in porous reservoirs: influence of reservoir factors and engineering choices on deliverability and storage operations. Int. J. Hydrogen Energy 49, 1088–1107. https://doi.org/10.1016/ i.iihvdene.2023.07.073.
- Chen, J.W., Fan, W., Bingham, B., et al., 2013. A long gravity-piston corer developed for seafloor gas hydrate coring utilizing an in situ pressure-retained method.

- Energies 6 (7), 3353-3372. https://doi.org/10.3390/en6073353.
- Chowdhury, M.A., Reza, M.S., Hossain, N., et al., 2021. Improvement of corrosion resistance of galvanization/nickel/chrome plating low carbon steels in H₂SO₄ under dynamic condition. Surf. Topogr. Metrol. Prop. 9 (3), 035018. https://doi.org/10.1088/2051-672X/ac19f0.
- Chu, Z.X., Dong, K.J., Gao, P.H., et al., 2021. Mine-oriented low-enthalpy geothermal exploitation: a review from spatio-temporal perspective. Energy Convers. Manag. 237, 114123. https://doi.org/10.1016/j.enconman.2021.114123.
- Dos Santos, C.A.L., Panossian, Z., 2019. Permanent rare-earth magnets—the need to protect them against corrosion. Mater. Sci. Appl. 10 (4), 317–327. https://doi.org/10.4236/msa.2019.104024.
- Fu, Q., Wang, G.R., Zhou, S.W., et al., 2020. Development of marine natural gas hydrate mining technology and equipment. Strategic Stud Chinese Acad. Eng. 22 (6), 32–39. https://doi.org/10.15302/J-SSCAE-2020.06.005.
- Gao, M.Z., Chen, L., Fan, D., et al., 2021. Principle and technology of coring with insitu pressure and gas maintaining in deep coal mine. J. China Coal Soc. 46 (3), 885–897. https://doi.org/10.13225/j.cnki.jccs.YT21.0297 (in Chinese).
- Gao, M.Z., Hao, H.C., Xue, S.N., et al., 2022. Discing behavior and mechanism of cores extracted from Songke-2 well at depths below 4,500 m. Int. J. Rock Mech. Min. Sci. 149, 104976. https://doi.org/10.1016/j.ijrmms.2021.104976.
- Gao, Y.M., Bai, Y., Zhu, H., et al., 2021. Corrosion resistance, mechanical and magnetic properties of cold-sprayed al coating on sintered NdFeB magnet. J. Therm. Spray Technol. 30 (8), 2117–2127. https://doi.org/10.1007/s11666-021-01266-z.
- Gladenkov, A.Y., Gladenkov, Y.B., 2021. Experience of deep-sea drilling in the world ocean: methodical and practical significance for stratigraphic studies. Stratigr. Geol. Correl. 29 (5), 548–571. https://doi.org/10.1134/S0869593821050026.
- Gong, J.M., Qiu, Z., Zou, C.N., et al., 2020. An integrated assessment system for shale gas resources associated with graptolites and its application. Appl. Energy 262, 114524. https://doi.org/10.1016/j.apenergy.2020.114524.
- Guo, D., Xie, H.P., Chen, L., et al., 2023a. In-situ pressure-preserved coring for deep exploration: insight into the rotation behavior of the valve cover of a pressure controller. Petrol. Sci. 20 (4), 2386–2398. https://doi.org/10.1016/ j.petsci.2023.02.020.
- Guo, D., Xie, H.P., Gao, M.Z., et al., 2023b. In-situ pressure-preserved coring for deep oil and gas exploration: design scheme for a coring tool and research on the insitu pressure-preserving mechanism. Energy 286, 129519. https://doi.org/ 10.1016/j.energy.2023.129519.
- He, Z.Q., Chen, L., Lu, T., et al., 2019. The optimization of pressure controller for deep earth drilling. Therm. Sci. 23 (Suppl. 3), 877–885. https://doi.org/10.2298/TSCI180612123H.
- Högberg, S., Holbøll, J., Mijatovic, N., et al., 2016. Direct reuse of rare earth permanent magnets—coating integrity. IEEE Trans. Magn. 53 (4), 1–9. https://doi.org/10.1109/TMAG.2016.2636804.
- Hou, W.T., Wang, H.P., Yuan, L., et al., 2021. Experimental research into the effect of gas pressure, particle size and nozzle area on initial gas-release energy during gas desorption. Int. J. Min. Sci. Technol. 31 (2), 253–263. https://doi.org/10.1016/j.ijmst.2021.01.002.
- Hu, J.J., Xie, H.P., Sun, Q., et al., 2021. Changes in the thermodynamic properties of alkaline granite after cyclic quenching following high temperature action. Int. J. Min. Sci. Technol. 31 (5), 843–852. https://doi.org/10.1016/j.ijmst.2021.07.010.
- Hu, Z.Q., Zhang, Y., Zeng, Y., 2023. Controlling effects of cap rocks on the formation of deep geothermal resources. Energy Geosci. 4 (4), 100208. https://doi.org/ 10.1016/j.engeos.2023.100208.
- Isotahdon, E., Huttunen-Saarivirta, E., Heinonen, S., et al., 2015. Corrosion mechanisms of sintered Nd—Fe—B magnets in the presence of water as vapour, pressurised vapour and liquid. J. Alloys Compd. 626, 349—359. https://doi.org/10.1016/j.jallcom.2014.12.048.
- Isotahdon, E., Huttunen-Saarivirta, E., Kuokkala, V., et al., 2014. Corrosion protection provided by electrolytic nickel and tin coatings for Nd–Fe–B magnets. J. Alloys Compd. 585, 203–213. https://doi.org/10.1016/j.jallcom.2013.09.135.
- Kubo, Y., Mizuguchi, Y., Inagaki, F., et al., 2014. A new hybrid pressure-coring system for the drilling vessel Chikyu. Sci. Drill. 17 (17), 37–43. https://doi.org/10.5194/ sd-17-37-2014.
- Kvenvolden, K.A., Cameron, D.H., 1983. Pressure core barrel: application to the study of gas hydrates, deep sea drilling Project site 533, leg 76. Initial Rep. DSDP 76, 367–375. https://doi.org/10.2973/dsdp.proc.76.107.1983.
- Li, C., Xie, H.P., Gao, M.Z., et al., 2021. Novel designs of pressure controllers to enhance the upper pressure limit for gas-hydrate-bearing sediment sampling. Energy 227 (5), 1–15. https://doi.org/10.1016/j.energy.2021.120405.
- Li, J.N., Wang, J., Hu, Y.Q., et al., 2022. Contact performance analysis of pressure controller's sealing interface in deep in-situ pressure-preserved coring system. Petrol. Sci. 19 (3), 1334–1346. https://doi.org/10.1016/j.petsci.2021.11.022.
- Li, X.T., Liu, W.Q., Yue, M., et al., 2017. Corrosion evaluation for recycled Nd-Fe-B sintered magnets. J. Alloys Compd. 699, 713–717. https://doi.org/10.1016/j.jallcom.2017.01.022.
- Liu, G.K., Gao, M.Z., Yang, Z.W., et al., 2020. The innovative design of deep in situ pressure retained coring based on magnetic field trigger controller. Adv. Civ. Eng. 2020, 8873628. https://doi.org/10.1155/2020/8873628.
- Liu, G.K., Li, C., You, Z.X., et al., 2023. Principle and technology of in-situ magnetically controlled multidirectional pressure-preserved coring in the coal mine. Coal Geol. Explor. 51 (8), 13–20. https://doi.org/10.12363/issn.1001-1986.22.12.0935 (in Chinese).
- Pasquale, V., Verdoya, M., Chiozzi, P., 2014. Heat flow and geothermal resources in northern Italy. Renew. Sustain. Energy Rev. 36, 277–285. https://doi.org/ 10.1016/j.rser.2014.04.075.

- Pettigrew, T.L., 1992. Design and operation of a wireline pressure core sampler (PCS). Ocean Drilling Program Tech. Notes 17, 1–43. https://doi.org/10.2973/odn.tn.17.1992
- Qin, W.Z., He, J., 2013. Research on composite powder and magnet properties of bonded NdFeB magnets prepared by press molding. Appl. Mech. Mater. 345, 218–222. https://doi.org/10.4028/www.scientific.net/AMM.345.218.
- Ren, H., 2020. Current status and development recommendations for gas hydrate sampling technology in the South China Sea. Petroleum Drilling Tech. 48 (4), 89–93. https://doi.org/10.11911/syztjs.2020045 (in Chinese).
- Sun, S.Q., Zhang, Q., Long, W.C., et al., 2019. Accurate test technology and device for coal seam gas content in long boreholes in underground coal mines. Coal Geol. Explor. 47 (4), 1–5, 1001-1986.2019.04-0001-05 (in Chinese).
- Thomas, C., Phillips, S.C., Flemings, P.B., et al., 2020. Pressure coring operations during the university of Texas-gulf of Mexico 2-1 (ut-gom2-1) hydrate pressure coring expedition in green canyon block 955, northern gulf of Mexico. AAPG (Am. Assoc. Pet. Geol.) Bull. 104 (9), 1877–1901. https://doi.org/10.1306/02262019036
- Tu, Q.Y., Cheng, Y.P., Xue, S., et al., 2021. Energy-limiting factor for coal and gas outburst occurrence in intact coal seam. Int. J. Min. Sci. Technol. 31 (4), 729–742. https://doi.org/10.1016/j.ijmst.2021.05.009.
- Wang, H.G., Huang, H.C., Bi, W.X., et al., 2022. Deep and ultra-deep oil and gas well drilling technologies: progress and prospect. Nat. Gas. Ind. B 9 (2), 141–157. https://doi.org/10.1016/j.ngib.2021.08.019.
- Wang, H., Wang, E.Y., Li, Z.H., et al., 2021. Study and application of a new gas pressure inversion model in coal seam while drilling based on directional drilling technology. Fuel 306, 1–15. https://doi.org/10.1016/j.fuel.2021.121679.
- Wang, J.L., Sun, Y., Qian, D.L., et al., 2022a. Scheme design and performance analysis of thin-walled pressure-retaining coring tools for seafloor drills in the deep-sea operating environment. J. Petrol. Sci. Eng. 208, 109790. https://doi.org/10.1016/i.petrol.2021.109790.
- Wang, J.L., Yu, M.F., Qian, D.L., et al., 2022b. Optimisation of drainage performance of the thin-walled core barrel sealing technology for pressure preservation sampling. Ocean. Eng. 250, 110996. https://doi.org/10.1016/j.oceaneng.2022.110996.
- Wang, X.G., Zou, D.Y., Yang, L.W., et al., 2020. Design of a pressure preservation coring tool for deep and ultra-deep coalbed methane samples. China Petroleum Machine 48 (1), 40–45. https://doi.org/10.16082/j.cnki.issn.1001-

- 4578.2020.01.006 (in Chinese).
- Wang, X.G., Zou, D.Y., Yang, L.W., et al., 2021. Development and field application of a coalbed methane coring tool with pressure maintenance, thermal insulation, and shape preservation capabilities. Petroleum Drilling Tech. 49 (3), 94–99. https://doi.org/10.11911/syztjs.2021061 (in Chinese).
- Xi, W., Liu, W.Q., Hu, R.J., et al., 2020. Property enhancement of bonded Nd-Fe-B magnets by composite adhesive design. Mater. Des. 192, 108767. https://doi.org/10.1016/j.matdes.2020.108767.
- Xie, H.P., Gao, F., Ju, Y., et al., 2017. Novel idea and disruptive technologies for the exploration and research of deep earth. Adv. Eng. Sci. 1 (49), 1–8. https://doi.org/10.15961/i.isuese.2017.01.001 (in Chinese).
- Xie, H.P., Gao, M.Z., Zhang, R., et al., 2020. Study on concept and progress of in situ fidelity coring of deep rocks. Chin. J. Rock Mech. Eng. 39 (5), 865–876. https:// doi.org/10.13722/i.cnki.jrme.2020.0138 (in Chinese).
- Xie, H.P., Li, C., He, Z., et al., 2021a. Experimental study on rock mechanical behavior retaining the in situ geological conditions at different depths. Int. J. Rock Mech. Min. Sci. 138, 104548. https://doi.org/10.1016/j.ijrmms.2020.104548.
 Xie, H.P., Liu, T., Gao, M.Z., et al., 2021b. Research on in-situ condition preserved
- Xie, H.P., Liu, T., Gao, M.Z., et al., 2021b. Research on in-situ condition preserved coring and testing systems. Petrol. Sci. 18 (6), 1840–1859. https://doi.org/ 10.1016/j.petsci.2021.11.003.
- Yang, L.W., Su, Y., Luo, J., et al., 2020. Development and application of GW-CP194-80A pressure-maintaining coring tool. Nat. Gas. Ind. 40 (4), 91–96. https://doi.org/10.3787/j.issn.1000-0976.2020.04.011 (in Chinese).
- Yang, Y.W., Jiang, N., Sun, Y.Z., et al., 2023. Structure and corrosion resistance characteristics of ZnAl/EP coating on bonded NdFeB magnet. J. Mater. Eng. Perform. 32 (12), 5475–5482. https://doi.org/10.1007/s11665-022-07472-2.
- Yao, B.H., Ma, Q.Q., Wei, J.P., et al., 2016. Effect of protective coal seam mining and gas extraction on gas transport in a coal seam. Int. J. Min. Sci. Technol. 26 (4), 637–643. https://doi.org/10.1016/j.ijmst.2016.05.016.
- Zhou, S.W., Zhang, J.H., Zou, C., et al., 2022. A new method for testing shale gas content based on pressure-holding coring technology. J. China Coal Soc. 47 (4), 1637–1646. https://doi.org/10.13225/j.cnki.jccs.2021.0249 (in Chinese).
- Zou, C.N., Ma, F., Pan, S.Q., et al., 2022. Earth energy evolution, human development and carbon neutral strategy. Petrol. Explor. Dev. 49 (2), 468–488. https://doi.org/10.1016/S1876-3804(22)60040-5.